Quantum Dot Patterning and Encapsulation by Maskless Lithography for Display Technologies

Resul Ozdemir, Hannes van Avermaet, Onur Erdem, Pieter Schiettecatte, Zeger Hens, Tangi Aubert

HAL is a multi-disciplinary open access archive for the deposit and dissemination of scientific research documents, whether they are published or not. The documents may come from teaching and research institutions in France or abroad, or from public or private research centers.

L'archive ouverte pluridisciplinaire **HAL**, est destinée au dépôt et à la diffusion de documents scientifiques de niveau recherche, publiés ou non, émanant des établissements d'enseignement et de recherche français ou étrangers, des laboratoires publics ou privés.

Quantum dot patterning and encapsulation by maskless lithography for display technologies
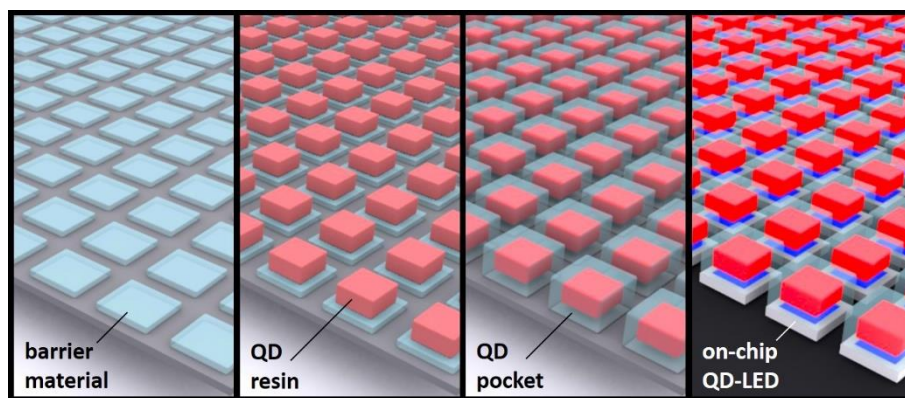
Resul Ozdemir[1], Hannes Van Avermaet[1], Onur Erdem[1], Pieter Schiettecatte[1], Zeger Hens[1*], Tangi Aubert[2*]

[1] Physics and Chemistry of Nanostructures, Ghent University, 9000 Gent, Belgium
[2] ICGM, University of Montpellier, CNRS, ENSCM, 34000 Montpellier, France

Emails: zeger.hens@ugent.be, tangi.aubert@umontpellier.fr

TOC graphic

Abstract
For their unique optical properties, quantum dots (QDs) have been extensively used as light emitters in a number of photonic and optoelectronic applications. They even met commercialization success through their implementation in high-end displays with unmatched brightness and color rendering. For such applications, however, QDs must be shielded from oxygen and water vapor, which are known to degrade their optical properties over time. Even with highly qualitative QDs, this can only be achieved through their encapsulation between barrier layers. With the emergence of mini and microLED for higher contrast and miniaturized displays, new strategies must be found for the concomitant patterning and encapsulation of QDs, with sub-millimeter resolutions. To this end, we developed a new approach for the direct patterning of QDs through maskless lithography. By combining QDs in photopolymerizable resins with digital light processing (DLP) projectors, we developed a versatile and massively parallel fabrication process for the additive manufacturing of functional structures that we refer to as QD pockets. These 3D heterostructures are designed to provide isotropic encapsulation of the QDs, and hence prevent edge ingress from the lateral sides of QD films, which remains a shortcoming of the current technologies.

Keywords
Semiconductor nanocrystals, surface chemistry, QD-LED, blade coating, 3D printing, stereolithography SLA

1. Introduction

Colloidal quantum dots (QDs) have emerged as a unique color converting material for lighting and display applications that can turn the blue light of a pump LED into any spectrum of colors for the realization of so-called QLED[1]. In particular, the possibility to finely tune the color of the re-emitted light makes QDs stand out with respect to more traditional powder phosphors based on lanthanide

ions. In recent developments of this technology, it was demonstrated that QDs are best deposited directly on top of a blue LED chip[2]. This so-called on-chip approach offers more design flexibility and requires less QDs than the established remote-phosphor approach, in which the QDs are distanced from the blue chip to reduce photothermal degradation. This on-chip approach is getting even more popular with the emergence of mini and microLEDs, which are expected to play a major role in the future of display technologies[3].

The fabrication of on-chip QLED requires depositing QDs following well-defined patterns and, in the case of microLED applications, with micron-scale resolution. To this end, a variety of techniques have been developed for the dispensing and patterning of QD materials[3]. Jetting techniques, for instance, including ink jetting[4] and aerosol jetting[5], have been used for QLED fabrication. However, being serial methods, the fabrication capabilities of these techniques are limited by the number of printing heads. Direct photolithography techniques have also been developed for the localized reticulation of QD films under UV light patterns[6,7], offering high resolution and good parallelization. However, these techniques require the manufacturing of a physical mask for each pattern, which is onerous and may hamper the implementation and versatility of the fabrication process.

Besides patterning, another challenge associated with on-chip QLED involves preventing any deterioration of the light emitters over time. The on-chip configuration exposes QDs to a considerable flux of blue light and elevated temperature, both of which accelerate the photochemical degradation of QDs by oxygen and water vapor[8]. This degradation can be mitigated by encapsulating QDs with oxygen and water vapor barrier layers. In current technologies, this is mostly achieved through thin film encapsulation (TFE)[9,10]. In TFE, a hybrid coating of QDs dispersed in an organic matrix is capped by multiple alternating organic and inorganic barrier layers. However, even with the best performing barriers, the resulting stack suffers from edge effects, with oxygen and water vapor penetrating at the sides of the thin film[11]. This edge ingress will inevitably be even more problematic for microLEDs since the edge proportion will increase with decreasing the lateral dimensions of the LED. Developing new encapsulation strategies is therefore essential for incorporation of QDs in lighting and display applications.

In this work, we propose a facile and versatile approach using UV digital light processing (DLP) projectors for the direct patterning of QD based materials via maskless lithography. DLP projectors employ digital micromirror devices (DMD) made of millions of mirrors, each of which can be individually addressed to switch on or off a projected pixel. Coupled with a UV LED, this allows for the rapid generation of light patterns of virtually any shape. In addition, DLP projectors are more affordable and accessible than conventional photolithography tools that use physical masks. Thanks to these great benefits, DLP projectors are now one of the main spatial light modulators used in high-end stereolithography (SLA) 3D printers, with resolutions down to the micron scale[12,13].

A simple solution for QD-integration within direct photolithography approaches includes dispersing QDs in a dedicated photopolymer resin, a nanocomposite we will henceforth denote as QD-resin. However, highly emissive QDs are usually synthesized with aliphatic ligands whereas resins are typically blends of rather polar acrylate based monomers and crosslinkers. Simply dispersing QDs with common photolithography or stereolithography resins is therefore not straightforward and can result in aggregation or segregation of the QDs in the organic matrix[14]. As a result, direct photolithography or stereolithography of QDs has often been reported for water based systems[15,16], but such an approach is not compatible with the implementation of oxygen and water vapor barriers. In addition, although depositing thick films of resin by blade coating is relatively easy, maximizing the loading of a QD-resin is highly desirable in order to minimize the thickness of the color converting layer, while maintaining high optical densities. This holds true in particular for microLED, for which the thickness of the color convertor deposit should not exceed, by and large, the lateral dimensions of the underlying blue LED. To overcome these limitations, we started this work by modifying the QD surface in order to streamline their embedding in common resins. *Flash*-grown red-emitting CdSe/CdS QDs were chosen as a robust model system for the purpose of this demonstration[17–19]. Their coating with a silica shell further provided a platform for their straightforward in-situ functionalization with methacrylate groups, resulting in stable CdSe/CdS@SiO_2 nanoparticles in polar organic environment, and hence

2

enabling QD-resin formulations suitable for maskless lithography and even light-based 3D printing to be made.

Finally, through the processing of such photopolymerizable QD-resin by DLP, we conceived monolithic structures that we refer to as QD pockets, in which a QD-resin core is seamlessly encapsulated in all directions with a protective layer, hence preventing any edge ingress of oxygen or water vapor. Given the intrinsic design versatility – including dimensions, shapes and array patterns – of the DLP fabrication process, QD pockets may offer a single solution for all on-chip QLED applications, both for general and specialty lighting and for mini and microLED display technology.

2. Experimental section

2.1. Synthesis and surface functionalization of the CdSe/CdS@SiO$_2$ nanoparticles. The CdSe/CdS core-shell QDs were synthesized based on the seeded-growth *flash* method[17,18]. Full details on the QD synthesis are provided in the Supporting Information. The silica encapsulation of these QDs and their subsequent functionalization with methacrylate groups was performed via a one-pot reverse microemulsion process adapted from previously described procedures[19,20]. In a round-bottom flask, 18 nmol of QDs were dispersed in a mixture of 80 mL of heptane and 30 mL of Brij L4 surfactant. After 5 minutes under stirring, 4.5 mL of a 5 % ammonia solution in water was added to the mixture. After 1 h under stirring, 180 µL of tetraethyl orthosilicate (TEOS) was added to the mixture. After 3 days under stirring, 180 µL of a methacrylate-silane precursor, 3-(trimethoxysilyl)propyl methacrylate, was added and the reaction was left to proceed under stirring for one more day. The nanoparticles were then collected and washed with ethanol using centrifugal concentrators (VivaSpin20, 100 kDa MWCO). Finally, the nanoparticles were dispersed and stored in ethanol. The concentration of the QD@SiO$_2$ nanoparticles was determined by UV-vis absorption measurements, based on their absorbance at 300 nm and 350 nm, and using the corresponding intrinsic absorption coefficients of the QDs, which were calculated from the Maxwell-Garnett effective medium theory[21,22].

2.2. QD-resin formulation. To prepare the QD-loaded resins, a calculated amount of the QD@SiO$_2$ nanoparticle solution was placed in a vial and most of the ethanol was evaporated with an airflow. A commercial UV resin (Anycubic Clear) was added and the mixture was stirred to obtain a homogeneous suspension. The resin was then degassed under vacuum in order to remove remaining ethanol. The volume fraction (vol%) of the QDs in the QD-resin was estimated based on the volume of CdSe/CdS QDs only, i.e. the volume of silica is not included in this parameter, with the average volume of one QD being determined from transmission electron microscopy (TEM) images.

2.3. Resin casting and printing. The blank or QD-loaded resins were casted on glass slides by blade coating using a micrometer film applicator with an adjustable gap size from 0 to 8 mm with 10 µm increment, and coupled to a TQC Sheen Automatic Film Applicator operated at 20 mm/s. Immediately after deposition, the resin film was locally cured using a custom-built printing platform comprising a Wintech PRO4710 DLP projector based on a 1080p orthogonal DMD, and integrating a 385 nm LED with adjustable optical power densities in the range 5 - 25 mW cm^{-2}. The projector is equipped with a 92 mm working distance lens for a projected pixel size of 36 µm. Further details on the QD pockets printing platform and its operation are described in the result section. The 3D boat model, known as 3DBenchy, was obtained from Creative Tools and printed on an Anycubic Photon S printer with 50 µm layers and 8 seconds of exposure per layer.

2.4. Characterization methods. TEM images were acquired using a JEOL 1400flash operated at 100 kV. SEM images were acquired using a JEOL JSM 7600F operated at 2 kV, after metallization of the samples with a thin layer of gold. Stereomicroscopy fluorescence and reflection images were acquired using a Leica MZ10F microscope with a 1× air objective and equipped with a Leica DFC7000T color camera. The reflection images were acquired using an internal LED illumination. For fluorescence images, the samples were illuminated with an external UV LED (395 nm) and the emission was collected through a

420 nm low-pass filter. The fluorescence images were processed with ImageJ software to determine intensity profiles and integrated intensities. In those cases, only the red channel of the color image was used. Optical transmission microscopy images were acquired using a Leitz Laborlux microscope with a 10× air objective. The thickness of the printed layers was measured using a VeeCo Dektak 150 surface profiler. UV-vis absorption spectra were acquired with a PerkinElmer Lambda 950 UV-vis spectrophotometer. Photoluminescence spectra were acquired with a Edinburgh Instruments FLSP920 spectrophotometer with an excitation wavelength of 450 nm. Absolute photoluminescence quantum yields (PLQYs) of the QD solutions and the QD-resin film were determined using an integrating sphere for an excitation wavelength of 420 nm and using the two measurements method[23].

3. Results and discussion

3.1. QD-resins for light-based printing.

The particular QDs synthesized for this work consisted of a 3.7 nm CdSe core with a 2.9 nm thick CdS shell, for a total diameter of 9.5 nm (Figure 1a,b). During the reverse microemulsion process used for the growth of the silica shell, the native oleic acid ligands of the QDs are replaced by hydrolyzed silica monomers[24,25]. This method further allows for a direct control on the silica shell thickness[26]. In this case, the silica layer was purposefully kept rather thin, about 1-2 nm (inset Figure 1b), to minimize the volume of non-optically active inorganic material in subsequent composite QD-resin formulations. The surface functionalization with methacrylate-silane resulted in CdSe/CdS@SiO$_2$ nanoparticles with high colloidal stability in organic solvents. In contrast, similar nanoparticles with bare silica surface tend to aggregate and settle rapidly[20]. Thanks to the silica coating and methacrylate functionalization, the nanoparticles could readily be dispersed in a commercial UV resin specially designed for light-based 3D printing. For this work, we chose a colorless clear resin (Anycubic Clear) to avoid absorption of the light emitted by the QDs. After evaporation of the nanoparticles solvent, the resulting QD-resin preserves the original resin properties and can be directly used with a SLA-type 3D printer. The part in Figure 1c was printed on an Anycubic Photon S, which is an economical printer that uses a 405 nm LCD screen as spatial light modulator. For this print, we used standard settings, namely a layer thickness of 50 μm with an exposure time per layer of 8 seconds, and the part came out fine without any need for optimization. The part appeared homogeneous with evenly distributed QDs, which retained their photoluminescence properties (inset Figure 1c). Thus, this strategy of silica encapsulation may provide a direct approach for the integration with 3D printing of a variety of nanocrystals and nanomaterials with native aliphatic ligands, which otherwise may suffer from incompatibility with off-the-shelf UV curable resins.

3.2. Photo-patterning of QDs by DLP

The UV curable QD-resin formulation discussed above, can also be used for the patterning of QDs by direct photolithography without the need for protective layers and etching steps. In that regards, DLP projectors come as a versatile solution for the quick and easy generation of UV light patterns for maskless lithography. We designed a printing setup (Figure 1d) using a DLP projector with an orthogonal DMD offering over 2 million pixels (1920×1080p). Based on the projection optics, the size of a single projected pixel is about 36 μm for a total available projection area of 68×38 mm. The DLP projector is mounted on a vertical translation lab jack for Z motion. The printing setup further comprises a sample stage with XY motion and a through hole. Finally, a USB microscope is placed under the sample stage, which allows focusing the light pattern on the substrate. To this end, a fine UV pattern was projected on a glass slide coated with a cured continuous layer of QD-resin, and the red light emitted by the QDs was used to adjust the Z position. A set of alignment pins on the sample stage allows repositioning the substrate at the same place between the different layers during the fabrication process (vide infra, section 3.3). Nevertheless, the USB camera under the stage can also be used to correct for misalignment by adding marks on the back of the substrate.

To estimate the native printing resolution of this setup, a UV pattern consisting of individual pixels (Figure 1e) was projected on a layer of blank resin and the uncured material was removed by washing

with isopropanol. The transmission optical microscopy image in Figure 1f shows a good agreement of the printed material with the pattern, evidencing that the intrinsic resolution limit of the projector can be achieved. In addition, this resolution carries over large area with good homogeneity as observed by scanning electron microscopy (SEM) (Figure 1g). In Figure 1c, the 3D object was printed from a QD-resin with relatively low QD loading (< 0.01 vol%) for demonstration purposes. For optoelectronic applications, such as on-chip color convertors, high loadings of optically active material are required to reach the desired optical densities and, ideally, achieve full color conversion in thin films. To this end, a QD-resin formulation with a calculated QD fraction of 0.5 vol% was prepared by dispersing the corresponding amount of silica coated QDs in the resin as described in the experimental section. The actual QD fraction in the QD film was thereafter estimated through absorption spectroscopy and is discussed below together with the optical properties. Even with such a solid loading, the QD-resin could be cast on glass slides with the same parameters as the blank resin. On the other hand, QDs strongly absorb in the UV range and at such a high loading, they may compete with the photoinitiator (vide infra, section 3.4). Figure 2 shows the dependence of the size of single pixels printed from this high loading QD-resin as a function of the light dose. While low light doses (< 0.15 J/cm^2) resulted in printed pixels smaller than the actual projected pixel size, higher doses (> 0.18 J/cm2) caused over-curing with pixels larger than the projected pixel size. Therefore, in the following sections the light dose was kept to 0.16 J/cm^2 for QD-resin layers to avoid over-curing and maintain fidelity with the projected pattern.
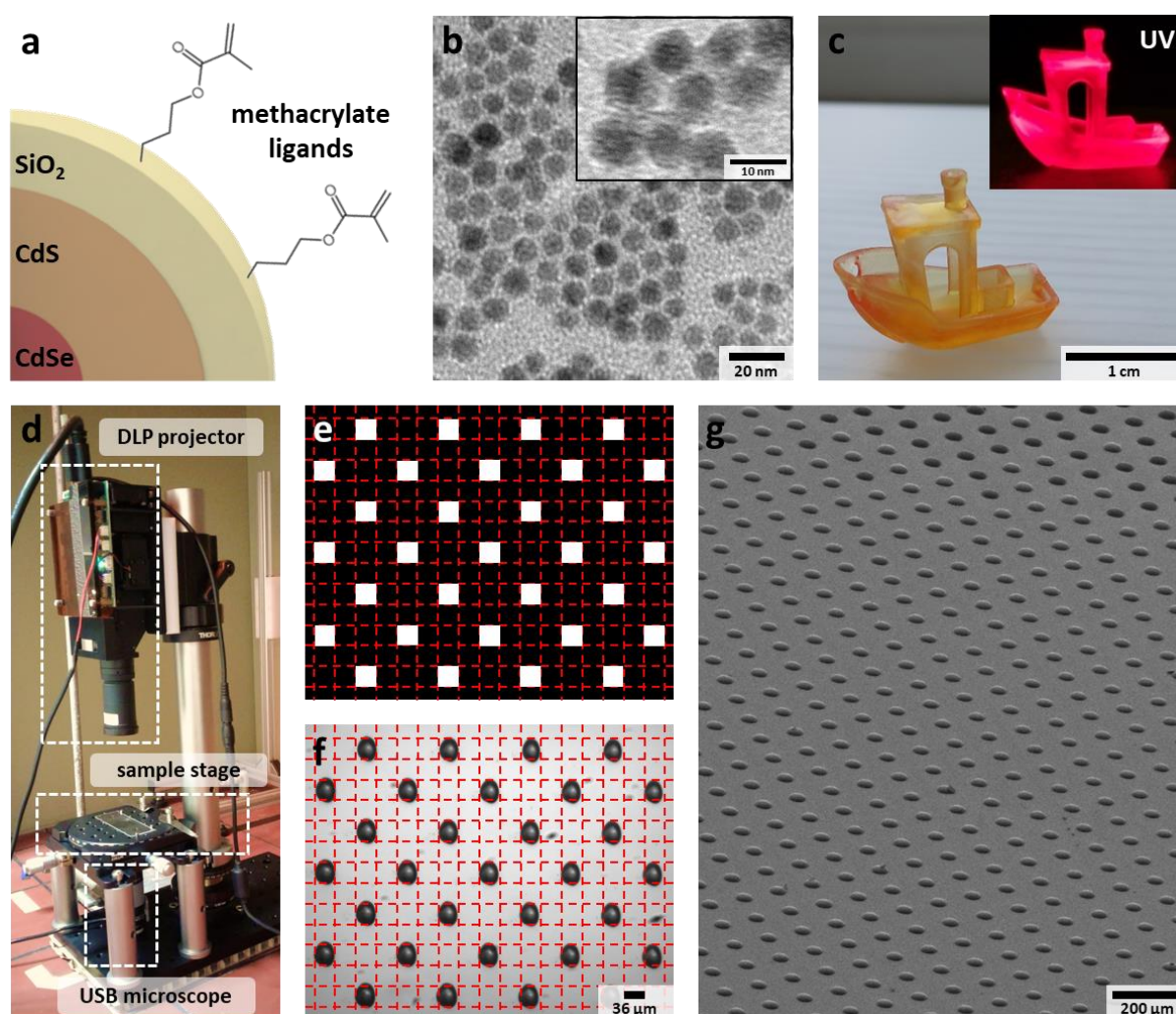
Figure 1. (a) Illustration of the methacrylate functionalized QD@SiO$_2$ nanoparticles. **(b)** TEM image of the CdSe/CdS QDs (inset: TEM image of the QD@SiO$_2$ nanoparticles). **(c)** Photograph of a 3D part printed from QD-resin (inset: photograph under UV illumination). **(d)** Photograph of the printing setup

developed for the patterning of QD and fabrication of QD pockets. **(e)** UV pattern, **(f)** optical transmission microscopy image, and **(g)** SEM image of a layer of individual pixels printed from blank resin. The red dashed lines in (e) and (f) outline the individual pixels of the projected pattern, which each correspond to one mirror of the DMD.
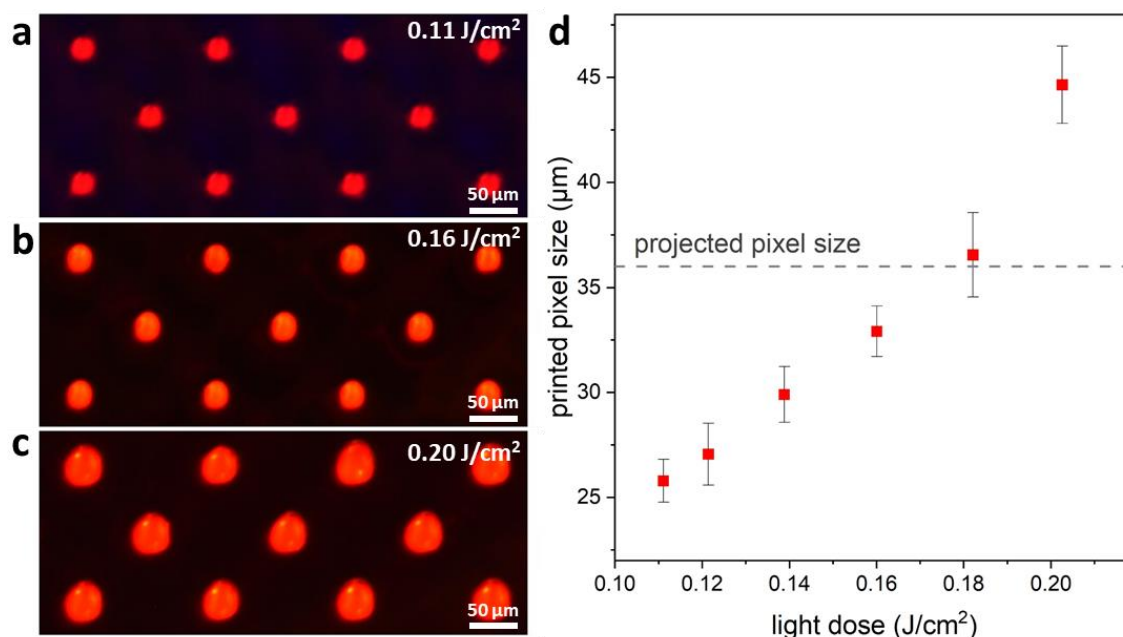

Figure 2. (a-c) Fluorescence images of single pixel patterns printed from 0.5 vol% QD-resin with light doses of 0.11, 0.16 and 0.20 J/cm^2, respectively. **(d)** Printed pixel size as function of the light dose (grey dashed line: theoretical projected pixel size; error bars: standard deviations on the printed pixel size). For all these prints the UV exposure time was kept to 10 s and the light dose was adjusted by changing the optical power density of the DLP projector.

3.3. Fabrication of QD pockets.

Besides the 2D patterning of QDs, the flexibility of the DLP projection system combined with the facile casting of QD-resin layers of several tens of µm also allows for the versatile fabrication of 3D heterostructures. Here, we demonstrate this through the fabrication of QD pockets. These pockets are designed so that the QD core is fully surrounded in all directions by a layer of blank resin, hence creating a seam-free barrier between the QD core and the surroundings. As illustrated in Figure 3, these QD pockets are fabricated by repeating three times the same printing steps of (1) casting the resin, (2) projecting the UV pattern, and (3) removing the uncured resin. A blank resin was used to print the base and top layers (Figures 3a, c), and a 0.5 vol% QD-resin was used to print the core layer (Figure 3b). The layers were formed atop each other by gradually increasing the gap height of the film applicator first by 30 µm above the substrate for the base layer, then by another 50 µm above the base for the core layer, and finally by 30 µm above the core for the top layer. The chosen patterns consisted in squares of 7×7 pixels for the base and top layers and 5×5 pixels for the core layer, for a total pocket lateral size of about 250 µm with a 36 µm wide protective wall surrounding the core. The base, core and top layers were printed with light doses of 0.09, 0.16 and 0.03 J/cm^2, respectively. While lower light doses are required for blank resin, early experiments showed that it should be adjusted in this case depending on film thickness. In brief, very thin layers require higher light dose for the pattern to be accurately printed. This could be due to the diffusion of oxygen in the resin, which is known to inhibit the photopolymerisation process[12]. The diffusion of oxygen after casting the resin should be more pronounced in thinner layers due to a higher surface to volume ratio. Thus, the light dose was accordingly increased for the base layer as compared to the top layer.

The fabrication process was followed layer-by-layer through contact stylus profilometry (Figure 4a) and stereomicroscopy (Figure 4b-d). The base, core and top layers show average thicknesses of 12 µm,

31 µm and 23 µm, respectively. For the core and top layers, the difference with the casting gap, which was 50 µm and 30 µm respectively, can be explained by the shrinkage of the organic matrix upon curing and removal of uncured material from the layer surface due to a higher oxygen content. For the base layer, the more pronounced deviation is most likely due to inaccurate calibration of the substrate height when setting the initial film applicator position. Next to height profiles, the reflection images (Figure 4b-d) further confirm that each layer also exhibits well-defined planar shapes. In Figure 4, both the surface profiles and reflection images show that the material surface has a tiled texture. This texture is caused by the small gaps between the mirrors that make the DMD, which inevitably create fine dark lines between the pixels of the UV pattern and hence result in lower light doses in those particular domains. In Figures 4b-d, this surface texture conveniently allows verifying the fidelity of the printed structure for the UV pattern simply by counting the number of printed pixels per pocket. For LED related applications, this surface texture may play a beneficial role in light outcoupling through scattering. Nevertheless, the QD pocket design also allows for the integration of volume scattering particles, such as TiO_2, which can be directly dispersed in the resin formulation of the top layer, in order to scatter light even more efficiently[27]. With this fabrication approach, non-planar top surfaces can even be considered, e.g. by forming a pyramidal structure, and hence optimize the light extraction[27]. If a flat and texture-free surface is desired for a particular application, a layer of resin can always be applied without any patterning step on top of the QD pocket or array of pockets after their device integration in order to smooth out this surface texturing.
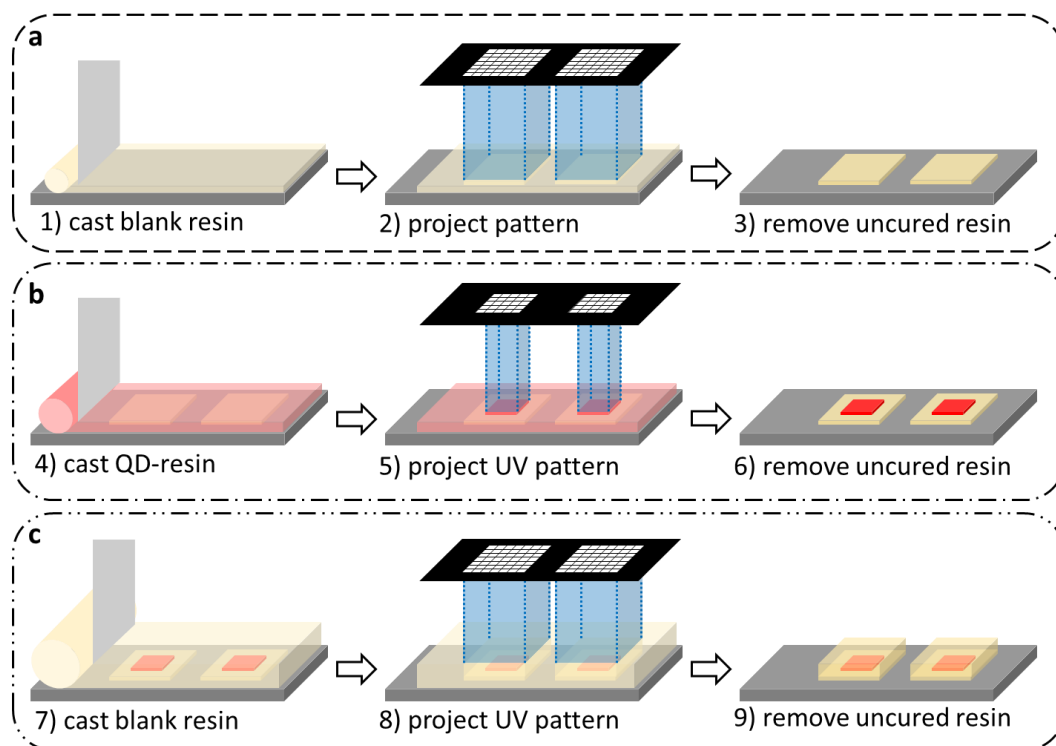
Figure 3. Illustration of the QD pockets fabrication process with the successive formations of **(a)** the base layer, **(b)** the core layer, and **(c)** the top layer.
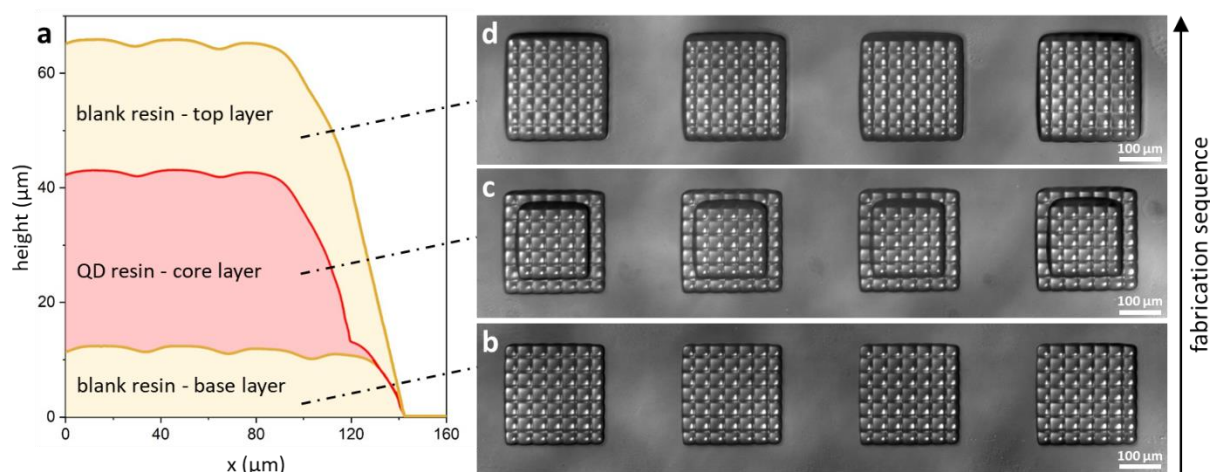
Figure 4. (a) Surface profilometry of the successive base, core and top layers. **(b-d)** Reflection images of the corresponding layers. In (b-d), greyscale images are displayed to highlight the sample topology.

In a fully formed QD pocket, the QD rich core is surrounded in all directions by a continuous layer of the same material. This creates a seamless barrier, free of any gap that would have inevitably resulted from an interface between different materials such as resin and glass. These QD pockets are therefore monolithic structures that are available from a source substrate and can be moved or manipulated. By adapting existing techniques, they could be transferred for instance by pick-and-place methods to a single blue LED for lighting applications or to an array of LEDs for microLED displays. In fact, QD pockets could be provided assembly-ready to process engineers. In particular, having QD pockets available in arrays, aligned with the eventual blue LED array, could enable a parallel transfer process that can strongly reduce production cost.

### 3.4. Optical properties of the QD pockets.

The color reflection and fluorescence images of the fully fabricated QD pockets (Figure 5a, b) clearly evidence the effective encapsulation of the QD core and the good homogeneity of the heterostructures. The photoluminescence coming from the pocket core is uniform as evidenced by the surface plot of a single pocket core (Figure 5c) and by the constant intensity profile across several pockets (Figure 5d). Besides the uniformity at single pocket level, it is also essential that all the pockets fabricated simultaneously on a large substrate share identical optical properties. The photoluminescence intensity of 190 different pockets analyzed over an area of 40 mm^2 (Figure S1) showed a standard deviation of only 8%, hence confirming the potential for large-scale production of pockets. To further characterize the QD dispersion, a large continuous QD-resin film was printed on a blank resin base to mimic the pocket configuration, while allowing for standard UV-vis spectroscopy measurements (Figure 6a). Figure 6b shows a good match between the absorption spectra of the QDs in solution and the QDs in film after subtracting the contribution from the resin itself. The deviation between QD film and solution at high energies could be due to a difference in the dielectric function of the QD environment[22]. The absence of light scattering from the QD-resin film, which could have been a sign of particle aggregation, is a good evidence of the homogeneous dispersion of the silica coated QD nanoparticles in the resin. Surface functionalization with methacrylate ligands is further promoting cross-linking between the nanoparticles and the resin, hence preventing segregation after curing. At 450 nm, which is the typical wavelength of blue LEDs used in lighting and display devices, the optical density of the QDs is about 0.5, which correspond to 70% absorption, with a contribution from the resin of only 2% to the optical density. As this was achieved with a 30 μm core, it leaves plenty of room to further increase the QDs optical density by increasing the pocket core thickness and/or loading.

The actual QD fraction in the film was estimated from the QD absorption spectrum (Figure 6b) and intrinsic absorption coefficient ($\mu_{300} = 188113$ cm^{-1}, $\mu_{350} = 125301$ cm^{-1}) calculated from the Maxwell-

8

Garnett effective medium theory for the specific ratio between the CdSe core and CdS shell volumes[21,22]. The experimental QD fraction in the film was found to be ca. 0.7 vol%, which is in good agreement with the calculated 0.5 vol% of the QD-resin and the shrinking of the film upon curing (see profilometry analysis, section 3.3). In line with the homogeneous fluorescence images of the pockets, the photoluminescence properties of the QDs remained unchanged after being embedded into resin and after printing. The small blue shift in emission observed between the QDs in solution and in film (Figure 6c) could be again due to a difference in the dielectric function of the environment rather than to self-absorption processes, which would have resulted in a red shift. In addition, the PLQY of the QDs during their processing was monitored through absolute measurements using an integrating sphere. The pristine QDs in toluene solution had a PLQY of 80%, which decreased to 58% after silica encapsulation and transfer into ethanol. Such a moderate decrease is often observed after stripping of native aliphatic ligands from QDs surface. Nevertheless, the QD resin film (Figure 6a) also showed a PLQY of 58%, indicating that the patterning process itself does not deteriorate the optical properties. On the other hand, drop casting the QD solutions directly on glass slides without resin resulted in PLQY of 31% for pristine QDs, and 40% for silica coated QDs. These more pronounced decreases in PLQY can reasonably be attributed to self-absorption and energy transfer processes between QDs due to their close proximity, especially for pristine QDs. It also highlights the benefice of dispersing the QDs in a resin film, which greatly suppresses these detrimental effects.
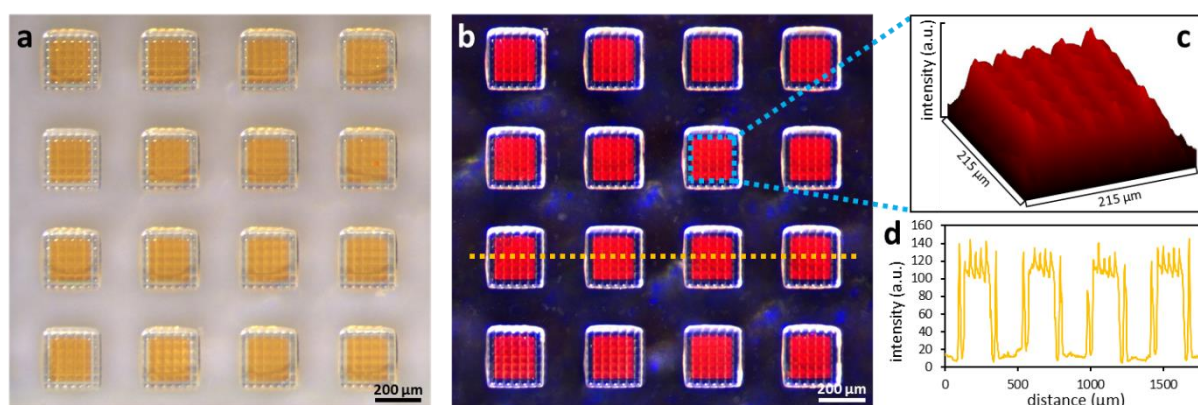
Figure 5. (a) Reflection image and **(b)** fluorescence image of QD pockets fabricated with 0.5 vol% QD-resin. **(c)** Surface plot of the fluorescence intensity over one pocket core. **(d)** Linear intensity profile across several pockets. In (b) the blue and orange dashed lines indicate the domains of analysis in (c) and (d), respectively. In (c) and (d) only the red color channel was used for the analysis.
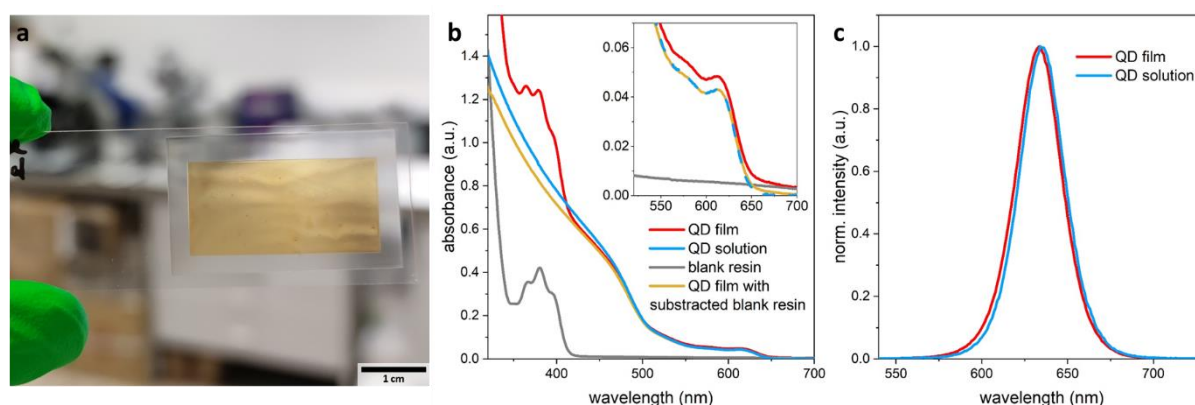

Figure 6. (a) Photograph of a continuous 0.5 vol% QD-resin film printed on top of a base layer of blank resin. **(b)** Absorption spectra of blank resin film, QD-resin film and the methacrylate functionalized QD@SiO$_2$ nanoparticles in ethanol solution. **(c)** Emission spectra of the QDs measured from the QD-resin film and from methacrylated QD@SiO$_2$ nanoparticles in ethanol.

9

3.5. A flexible fabrication method

A significant advantage of a fabrication process based on maskless lithography is the flexibility of DLP projectors, which allows for the facile and rapid variation of the directing pattern, hence allowing patterning in a desired shape. In addition, thanks to the millions of mirrors, i.e. pixels, which make the DMD, a large number of pockets can be printed in parallel; yet they can all be different from each other as well. Here, we demonstrate this flexibility through the fabrication of QD pockets of different sizes, different core and protective shell ratio, and different shapes (Figure 7). Since the printing resolution is governed by the projected pixel size, i.e. 36 µm with the DLP projector used in this work (Figure 1 and 2), the smallest pocket that could possibly be fabricated with this setup would consist of a 36 µm QD core surrounded by a 36 µm thick wall for the lateral dimensions. However, UV DLP projectors with advertised projected pixel sizes as low as 1 µm are readily available commercially, and some authors have reported sub-micrometer resolution for a DLP based fabrication process[13]. Another advantage of the DLP projector is the possibility to project grayscale patterns, hence allowing variation of the light dose within the same pattern. This is possible since the micromirrors do not remain static during projection. Instead, they continuously and rapidly switch from a neutral to an ON or OFF position. For instance, the projector used here can operate at 60 Hz to generate 8-bit grayscale patterns. We made use of this unique capability of DMDs to show that it is even possible to print structures with rounded or diagonal lines (Figure 7d). As illustrated in Figure S2, these geometries are possible by applying anti-aliasing to the pattern, creating pixels with lower gray values along the edges. Thanks to the lower light doses for those pixels, the printed structure can approximate the sub-pixel features.

In the context of on-chip color conversion applications, this fabrication flexibility will allow easy accommodation for the large variety of sizes and shapes of existing LEDs with minimum investment. This is a strong advantage over conventional photolithography, which requires the manufacturing of a specific physical mask for every possible configuration. In future developments, this approach should create new opportunities to conceive innovative device settings, for instance to optimize the packing of different colored pixels in next generation display technologies. In this context, Figure S3 illustrates how red- and green-emitting QD pockets can be printed side by side on the same substrate to facilitate their integration with blue LED arrays by, for instance, transfer printing. For the purpose of the demonstration, the pockets were printed on a simple glass slide, but the process may very well be applied to a variety of substrates including flexible substrates or even directly on top of a LED chip array.

The ambition of this work was hence to demonstrate the versatility of this QD patterning and encapsulation strategy, and to provide a proof-of-concept for the fabrication of 3D heterostructures such as the QD pockets. The next step for the development of these pockets will naturally be to evaluate the effective protection during prolonged operation. Such stability study, however, should be conducted next to the formulations and implementation of a resin with specific barrier properties for the outer layer. Here, a simple off-the-shelf resin with no particular barrier properties was used for the purpose of demonstrating the fabrication concept. Nevertheless, this encapsulation strategy would strongly benefit from the formulation of functional resins, for instance by integrating fillers with known barrier properties to oxygen and/or water vapor such as cellulose nanocrystals or nanoclay materials[28,29]. The implementation of such active barriers, should thereafter be investigated together with the optimization of the pocket design that may include varying the outer layer dimensions and enhancing light extraction. This aspect of technology development also brings out the need for new analytical tool for the evaluation of barrier properties at the scale of microLEDs. While monitoring the photoluminescence intensity over an array of QD pockets may provide some general information on stability, more localized visualizations of photoluminescence degradation would also be necessary to detect possible ingress through the barrier or via seams in the case of comparison with non-fully isotropic encapsulation. An option could be to combine the calcium test method with optical microscopy, by replacing the QD core with metallic Ca[30]. Considering that next generation mini and microLEDs are expected to have a transformative role in display technologies, we expect that the simultaneous development of adapted methodology for their characterization should also be the topic of important scientific efforts in the coming years.
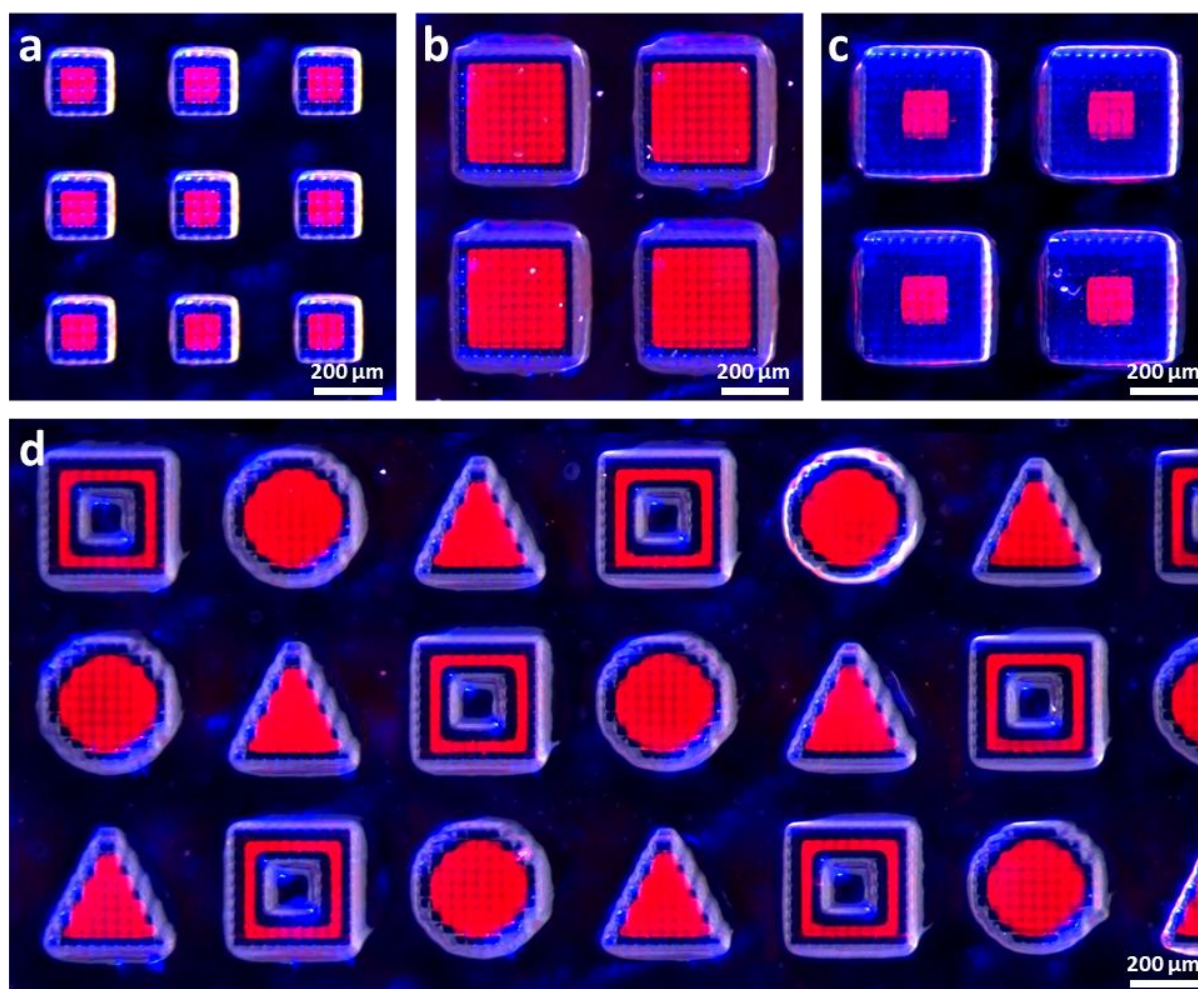
Figure 7. Fluorescence microscopy images of QD pockets with varying **(a-c)** dimensions and **(d)** shapes.

4. Conclusion

Overall, we propose a versatile and complete fabrication process, from the surface modification of nanocrystals for their integration with off-the-shelf photocurable resins, to their processing with accessible DLP projectors. While the 2D patterning of QDs is highly interesting for a number of photonic applications, we further demonstrated the possibility to quickly change the light pattern, which, together with the capability to cast macroscopic layers of the QD-resin, enables the fabrication of QD pockets. These 3D heterostructures were initially designed to protect the QDs from their environment and promote their implementation as on-chip light convertor for LED applications. Nevertheless, this pocket concept can also be applied to the encapsulation of other light emitters, such as organic dyes and inorganic phosphors, and more generally to any material that is prone to degradation and needs a protective barrier against it, to be used in applications such as micro-batteries and solar cells.

Supporting Information

The Supporting Information is available free of charge at https://pubs.acs.org
QDs synthesis details; Low magnification fluorescence image; Effect of grayscale pixels; Illustration of the fabrication process for QD-pockets with different colors.

References

(1) Jang, E.; Jun, S.; Jang, H.; Lim, J.; Kim, B.; Kim, Y. White-Light-Emitting Diodes with Quantum Dot Color Converters for Display Backlights. *Adv. Mater.* **2010**, *22* (28), 3076–3080.

(2) Shimizu, K. T.; Böhmer, M.; Estrada, D.; Gangwal, S.; Grabowski, S.; Bechtel, H.; Kang, E.; Vampola, K. J.; Chamberlin, D.; Shchekin, O. B.; Bhardwaj, J. Toward Commercial Realization of Quantum Dot Based White Light-Emitting Diodes for General Illumination. *Photonics Res.* **2017**, *5* (2), A1–A6.

(3) Liu, Z.; Lin, C.-H.; Hyun, B.-R.; Sher, C.-W.; Lv, Z.; Luo, B.; Jiang, F.; Wu, T.; Ho, C.-H.; Kuo, H.-C.; He, J.-H. Micro-Light-Emitting Diodes with Quantum Dots in Display Technology. *Light Sci. Appl.* **2020**, *9* (1), 83.

(4) Kong, Y. L.; Tamargo, I. A.; Kim, H.; Johnson, B. N.; Gupta, M. K.; Koh, T.-W.; Chin, H.-A.; Steingart, D. A.; Rand, B. P.; McAlpine, M. C. 3D Printed Quantum Dot Light-Emitting Diodes. *Nano Lett.* **2014**, *14* (12), 7017–7023.

(5) Han, H.-V.; Lin, H.-Y.; Lin, C.-C.; Chong, W.-C.; Li, J.-R.; Chen, K.-J.; Yu, P.; Chen, T.-M.; Chen, H.-M.; Lau, K.-M.; Kuo, H.-C. Resonant-Enhanced Full-Color Emission of Quantum-Dot-Based Micro LED Display Technology. *Opt. Express* **2015**, *23* (25), 32504–32515.

(6) Wang, Y.; Fedin, I.; Zhang, H.; Talapin, D. V. Direct Optical Lithography of Functional Inorganic Nanomaterials. *Science* **2017**, *357* (6349), 385.

(7) Hahm, D.; Lim, J.; Kim, H.; Shin, J.-W.; Hwang, S.; Rhee, S.; Chang, J. H.; Yang, J.; Lim, C. H.; Jo, H.; Choi, B.; Cho, N. S.; Park, Y.-S.; Lee, D. C.; Hwang, E.; Chung, S.; Kang, C.; Kang, M. S.; Bae, W. K. Direct Patterning of Colloidal Quantum Dots with Adaptable Dual-Ligand Surface. *Nat. Nanotechnol.* **2022**, *17* (9), 952–958.

(8) Moon, H.; Lee, C.; Lee, W.; Kim, J.; Chae, H. Stability of Quantum Dots, Quantum Dot Films, and Quantum Dot Light-Emitting Diodes for Display Applications. *Adv. Mater.* **2019**, *31* (34), 1804294.

(9) Park, J.-S.; Chae, H.; Chung, H. K.; Lee, S. I. Thin Film Encapsulation for Flexible AM-OLED: A Review. *Semicond. Sci. Technol.* **2011**, *26* (3), 34001.

(10) Chen, J.; Hardev, V.; Yurek, J. Quantum-Dot Displays: Giving LCDs a Competitive Edge through Color. *Inf. Disp. (1975).* **2013**, *29* (1), 12–17.

(11) Nelson, E. W.; McDaniel, D. J.; Eckert, K. L. Quantum Dot Applications in LCD Displays. *TechConnect Briefs* **2015**, *1*, 282–285.

(12) Tumbleston, J. R.; Shirvanyants, D.; Ermoshkin, N.; Januszewicz, R.; Johnson, A. R.; Kelly, D.; Chen, K.; Pinschmidt, R.; Rolland, J. P.; Ermoshkin, A.; Samulski, E. T.; DeSimone, J. M. Continuous Liquid Interface Production of 3D Objects. *Science* **2015**, *347* (6228), 1349.

(13) Sun, C.; Fang, N.; Wu, D. M.; Zhang, X. Projection Micro-Stereolithography Using Digital Micro-Mirror Dynamic Mask. *Sensor. Actuat. A-Phys.* **2005**, *121* (1), 113–120.

(14) Yang, K. P.; Son, S.-R.; Baek, S. H.; Lee, J. H.; Lee, K. Fabrication of Light Emitting Diodes Using Photo-Patternable Quantum Dot-Acrylate Resins. *J. Mater. Chem. C* **2021**, *9* (47), 17084–17088.

(15) Liu, S.-F.; Hou, Z.-W.; Lin, L.; Li, F.; Zhao, Y.; Li, X.-Z.; Zhang, H.; Fang, H.-H.; Li, Z.; Sun, H.-B. 3D Nanoprinting of Semiconductor Quantum Dots by Photoexcitation-Induced Chemical Bonding. *Science* **2022**, *377* (6610), 1112–1116.

(16) Pawar, A. A.; Saada, G.; Cooperstein, I.; Larush, L.; Jackman, J. A.; Tabaei, S. R.; Cho, N.-J.; Magdassi, S. High-Performance 3D Printing of Hydrogels by Water-Dispersible Photoinitiator Nanoparticles. *Sci. Adv.* **2016**, *2* (4), e1501381.

(17) Cirillo, M.; Aubert, T.; Gomes, R.; Van Deun, R.; Emplit, P.; Biermann, A.; Lange, H.; Thomsen, C.; Brainis, E.; Hens, Z. "Flash" Synthesis of CdSe/CdS Core–Shell Quantum Dots. *Chem. Mater.* **2014**, *26* (2), 1154–1160.

(18) Drijvers, E.; De Roo, J.; Geiregat, P.; Fehér, K.; Hens, Z.; Aubert, T. Revisited Wurtzite CdSe Synthesis: A Gateway for the Versatile Flash Synthesis of Multishell Quantum Dots and Rods. *Chem. Mater.* **2016**, *28* (20), 7311–7323.

(19) Aubert, T.; Soenen, S. J.; Wassmuth, D.; Cirillo, M.; Van Deun, R.; Braeckmans, K.; Hens, Z. Bright and Stable CdSe/CdS@SiO2 Nanoparticles Suitable for Long-Term Cell Labeling. *ACS Appl. Mater. Interfaces* **2014**, *6* (14), 11714–11723.

(20) Drijvers, E.; Liu, J.; Harizaj, A.; Wiesner, U.; Braeckmans, K.; Hens, Z.; Aubert, T. Efficient Endocytosis of Inorganic Nanoparticles with Zwitterionic Surface Functionalization. *ACS Appl. Mater. Interfaces* **2019**, *11* (42), 38475–38482.

(21) De Geyter, B.; Hens, Z. The Absorption Coefficient of PbSe/CdSe Core/Shell Colloidal Quantum Dots. *Appl. Phys. Lett.* **2010**, *97* (16), 161908.

(22) Hens, Z.; Moreels, I. Light Absorption by Colloidal Semiconductor Quantum Dots. *J. Mater. Chem.* **2012**, *22* (21), 10406–10415.

(23) Leyre, S.; Coutino-Gonzalez, E.; Joos, J. J.; Ryckaert, J.; Meuret, Y.; Poelman, D.; Smet, P. F.; Durinck, G.; Hofkens, J.; Deconinck, G.; Hanselaer, P. Absolute Determination of Photoluminescence Quantum Efficiency Using an Integrating Sphere Setup. *Rev. Sci. Instrum.* **2014**, *85* (12), 123115.

(24) Darbandi, M.; Thomann, R.; Nann, T. Single Quantum Dots in Silica Spheres by Microemulsion Synthesis. *Chem. Mater.* **2005**, *17* (23), 5720–5725.

(25) Koole, R.; van Schooneveld, M. M.; Hilhorst, J.; de Mello Donegá, C.; Hart, D. C.; van Blaaderen, A.; Vanmaekelbergh, D.; Meijerink, A. On the Incorporation Mechanism of Hydrophobic Quantum Dots in Silica Spheres by a Reverse Microemulsion Method. *Chem. Mater.* **2008**, *20* (7), 2503–2512.

(26) Biermann, A.; Aubert, T.; Baumeister, P.; Drijvers, E.; Hens, Z.; Maultzsch, J. Interface Formation during Silica Encapsulation of Colloidal CdSe/CdS Quantum Dots Observed by in Situ Raman Spectroscopy. *J. Chem. Phys.* **2017**, *146* (13), 134708.

(27) Karadza, B.; Van Avermaet, H.; Mingabudinova, L.; Hens, Z.; Meuret, Y. Comparison of Different RGB InP-Quantum-Dot-on-Chip LED Configurations. *Opt. Express* **2022**, *30* (24), 43522–43533.

(28) Wang, J.; Gardner, D. J.; Stark, N. M.; Bousfield, D. W.; Tajvidi, M.; Cai, Z. Moisture and Oxygen Barrier Properties of Cellulose Nanomaterial-Based Films. *ACS Sustain. Chem. Eng.* **2018**, *6* (1), 49–70.

(29) Majeed, K.; Jawaid, M.; Hassan, A.; Abu Bakar, A.; Abdul Khalil, H. P. S.; Salema, A. A.; Inuwa, I. Potential Materials for Food Packaging from Nanoclay/Natural Fibres Filled Hybrid Composites. *Mater. Des.* **2013**, *46*, 391–410.

(30) Nisato, G.; Klumbies, H.; Fahlteich, J.; Müller-Meskamp, L.; van de Weijer, P.; Bouten, P.; Boeffel, C.; Leunberger, D.; Graehlert, W.; Edge, S.; Cros, S.; Brewer, P.; Kucukpinar, E.; de Girolamo, J.; Srinivasan, P. Experimental Comparison of High-Performance Water Vapor Permeation Measurement Methods. *Org. Electron.* **2014**, *15* (12), 3746–3755.